
ANALYSIS OF CARDIAC ARRHYTHMIA SOURCES USING FEYNMAN DIAGRAMS

Louise Arno

KU Leuven Campus KULAK, Department of Mathematics: 8500 Kortrijk, Belgium
KU Leuven, iSi Health, Institute of Physics-based Modeling for In Silico Health: 3000 Leuven, Belgium

Desmond Kabus

KU Leuven Campus KULAK, Department of Mathematics: 8500 Kortrijk, Belgium
Leiden University Medical Center (LUMC), Laboratory of Experimental Cardiology: 2333ZA Leiden, the Netherlands
KU Leuven, iSi Health, Institute of Physics-based Modeling for In Silico Health: 3000 Leuven, Belgium

Hans Dierckx

KU Leuven Campus KULAK, Department of Mathematics: 8500 Kortrijk, Belgium
KU Leuven, iSi Health, Institute of Physics-based Modeling for In Silico Health: 3000 Leuven, Belgium
h.dierckx@kuleuven.be

July 6, 2023

ABSTRACT

The contraction of the heart muscle is triggered by self-organizing electrical patterns. Abnormalities in these patterns lead to cardiac arrhythmias, a prominent cause of mortality worldwide [WHO, 2020]. The targeted treatment or prevention of arrhythmias requires a thorough understanding of the interacting wavelets, vortices and conduction block sites within the excitation pattern. Currently, there is no conceptual framework that covers the elementary processes during arrhythmogenesis in detail, in particular the transient pivoting patterns observed in patients, which can be interleaved with periods of less fragmented waves [Rodrigo et al., 2017, Tabereaux et al., 2009, Seitz et al., 2017]. Here, we provide such a framework in terms of quasiparticles and Feynman diagrams, which were originally developed in theoretical physics.

We identified three different quasiparticles in excitation patterns: heads, tails and pivots. In simulations and experiments, we show that these basic building blocks can combine into at least four different bound states. By representing their interactions as Feynman diagrams [Feynman, 1949], the creation and annihilation of rotor pairs are shown to be sequences of dynamical creation, annihilation and recombination of the identified quasiparticles.

Our results provide a new theoretical foundation for a more detailed theory, analysis and mechanistic insights of topological transitions in excitation patterns, to be applied within and beyond the context of cardiac electrophysiology.

Keywords cardiac arrhythmia, Feynman diagram, data analysis, topology, excitable systems

1 Introduction

Gaining a better understanding of the complex processes at different spatiotemporal scales during heart rhythm disorders is a major challenge. The mechanical contraction of each myocyte in the heart is triggered by electrical depolarization of the cells, which first propagates through a dedicated conduction system, but is thereafter passed on from cardiomyocyte to cardiomyocyte. As a result, the activation wave can re-excite itself, or a local focal source can start extra excitations.

Such abnormal emerging behavior manifests as a cardiac arrhythmia. With a global mortality rate of 16% in 2019, and increasing numbers every year, cardiac arrhythmias remain one of the largest causes of death worldwide [WHO, 2020].

A simple arrhythmia in which the excitation wave follows a fixed path in time, or which originates from a region of ectopic impulse formation can be treated by ablation therapy, in which the trigger or path is physically destroyed [Haissaguerre et al., 1998]. Even though efficiency has improved significantly throughout the years, the success rate is rather low for arrhythmia with incompletely understood spatio-temporal organization [Cronin et al., 2019, Mujović et al., 2017]. Such arrhythmias include ventricular fibrillation [Gray et al., 1998, Jalife et al., 1998], which is the most lethal one, and atrial fibrillation, which affects approximately 1% of the world population, and is responsible for one third of stroke cases [Samol et al., 2016]. In both atrial and ventricular fibrillation, as well as in ventricular tachycardia, rotating vortices of activation have been observed [Allessie et al., 1973], named spiral waves, scroll waves or cardiac rotors. While computer simulations of the heart [Gray et al., 1995] and initial observations [Gray et al., 1998] often yield long-lived stable rotors, complex patterns detected in real hearts commonly show a more complex regime that exhibits conduction blocks and transient rotors which do not even complete a full turn. There is a consensus that interacting wave fragments, also called wavelets [Moe and Abildskov, 1959, Lee et al., 2020, Arno et al., 2021] play a role in atrial and ventricular fibrillation. However, the precise mechanisms of onset, sustainment and termination of complex arrhythmias remain to be further elucidated [Aras et al., 2017, Shibata et al., 2022].

The state-of-the-art analysis of complex conduction patterns in the heart wall relies on the periodic activation cycle of the cardiomyocytes, called the action potential. By mapping the electrical activity of each point of the heart onto a phase angle in the interval $[0, 2\pi]$, one obtains a phase map of the heart at a given time [Gray et al., 1998, Clayton et al., 2005]. After spatial filtering of the signal, distinct points occurred where all phases meet, called phase singularities [Gray et al., 1998]. Since then, analysis tools [Gray et al., 1998, Bray and Wikswo, 2003], ablation strategies [Narayan et al., 2012] and mathematical theory [Clayton et al., 2005, Panfilov and Dierckx, 2017] has been developed based on the assumed existence of phase singularities during arrhythmia.

This now-classical viewpoint was recently challenged independently by two groups, who noted that at the rotor core in simulations [Tomii et al., 2021, Arno et al., 2021] or experimental optical recordings [Arno et al., 2021], there is not a single point of ill-defined phase, but an entire line across which the phase changes abruptly. This was called a phase discontinuity or phase defect line. These locations are also known in classical literature as sites of conduction block [Janse et al., 1980] and are commonly detected by clinicians when they map local activation times. The aim of this paper is to provide a more detailed theoretical framework that reconciles the concepts of wave fronts, wave backs, conduction blocks, and rotors, with either steady or unsteady meandering cores, to unravel the critical processes that cause, sustain or terminate complex arrhythmias. We purposely use terminology from particle physics, as in this work we bring several analogies from that discipline to a cardiac context.

2 Conceptual framework

Our analysis method starts from an observed excitation pattern and uses a consistent visual language within this paper, see Fig. 1A.

First, the pattern are divided into three regions (see Fig. 1B): excited (E, yellow), unexcited (U, white) or phase defect (PD, black). The latter case happens where cells of distinct phase meet, which can occur e.g. due to a conduction block, a local stimulus, heterogeneous tissue properties, or in highly excitable media where rotors exhibit so-called linear cores [Krinsky et al., 1992, Tomii et al., 2021, Arno et al., 2021]. Where cells locally change from the unexcited to the excited state, one finds the classical wavefront (F, cyan). Conversely, where cells locally recover from being refractory, the wave back (B, magenta) is found.

We define three fundamental building blocks, so-called quasiparticles, as the end points of three different curves in the observed patterns. We call the end points of a wave front “heads”, the end points of a wave back “tails”, and the end points of a phase defect line “pivots”. Those special points are drawn in blue, red, and green, respectively. Since any non-closed curve ends in two points, the heads, tails, and pivots each come in pairs.

Seen from any position on a given wave front and looking towards the unexcited region, one head is found to the left, denoted as h^+ in Fig. 1C, and one is found to the right, denoted as h^- . Here, the black zone can not only represent a phase defect line, but also an inexcitable obstacle or points outside the myocardium. Considering the medium boundary also as a phase defect is required to guarantee that every front ends on two heads.

We endow the heads propagating in counterclockwise direction around the obstacle, or phase defect, with a positive “charge” $Q = +\frac{1}{2}$ and the clockwise $Q = -\frac{1}{2}$ respectively. The sign in the notation h^\pm refers to the sign of this charge. The value of $\pm\frac{1}{2}$ is chosen since in the high excitability regime, the change of activation phase across a wave front

will be half a cycle, i.e. $\pm\pi$. We make the convention that points on the medium boundary also carry this charge, from which it follows that the net charge over all heads in the medium is zero.

To the two tails connected by a wave back, we analogously ascribe a charge of $\pm\frac{1}{2}$ depending on their chirality, see Fig. 1C. Since this charge also logs a jump of $\pm\pi$ in the local activation phase, tail charges and head charges are of the same type, which we denoted above as charge Q . The charge value $\frac{1}{2}$ is the smallest one possible in our framework, much like the elementary charge e in physics.

The third building block, the pivot p is already being used by clinicians [Seitz et al., 2017]: Pivots are marked in maps of local activation time as the endpoint of a conduction block line. Mathematically, a pivot corresponds to a branch point of the activation phase surface [Tomii et al., 2021, Arno et al., 2021]. Wave fronts that initially travelled around the pivot in counterclockwise manner, are given a charge of $+\frac{1}{2}$, and $-\frac{1}{2}$ for clockwise rotation. Here $\frac{1}{2}$ refers to a half turn in *space*, rather than completing half an excitation cycle, as was the case for heads and tails. The pivot charge is thus different from the head or tail charge, and we denote it with P and in subscript: p_{\pm} . An overview of the different quasiparticles is given in the top rows of Fig. 1C and in Table. 1.

Strikingly, our analysis of activation patterns in simulation and experiments revealed that the three fundamental building blocks tend to form bound states, much like a hydrogen atom consists of a proton and an electron, or like a proton itself is made up of two up quarks and one down quark in particle physics.

So far, we discovered four bound states, see Fig. 1C and Table 1. The first one consists of a head and a tail of equal Q -charge. Already in Fig. 1B, it can be seen that while the tail traces a boundary or phase defect, the head will usually follow it directly, exciting the newly-recovered tissue created by the tail particle, such that they propagate as a pair along the phase defect, with a small excitable gap between them. In the classical viewpoint, this corresponds to a wave front and wave back ending in one point, the classical “spiral tip”. In three spatial dimensions, the tips form a filament curve [Winfree et al., 1996, Clayton et al., 2005] around which the wave rotates. Therefore, we annotate the bound state of head and tail with f and call it a filament point (purple). The convention of assigning half a Q -charge to heads and tails has the useful property that the sum of these charges will be equal to the classical topological charge $Q = \frac{1}{2} + \frac{1}{2} = 1$ of the filament. As the absolute charge of a filament particle is always the same, we abbreviate the “full” notation $f^{\pm\pm}$ to f^{\pm} , see second column in Tab. 1. In this simpler notation, we write the charges of all particles with superscript. For example, p^+ , rather than p_+ .

In simple computational models of excitable processes, an initial conduction block line as in Fig. 1B will only be transient, and quickly shrink to a small region where the wave front and wave back meet. Due to the conservation of Q and P charges over time, such region will have $Q = P = \pm 1$ and corresponds to the well-known regime of circular-core spiral waves. We call such state a ‘core particle’, denoted $c_{\pm\pm}^{\pm\pm}$ or shorter c^{\pm} and indicated by an orange circle.

The next two bound states have no classical counterpart to our knowledge. Consider a propagating wave front that hits a wave back. Such event will generally occur in a single point first, creating a small phase defect. The end point of one side of the wave front will then travel along the existing wave back, and in the process, the conduction block region grows to become a phase defect line. Hence, there exists a state of a head, tail, and pivot of the same chirality that all move together. We call this a “growth” particle and denote it with a black circle. It has $Q = \pm 1$ and $P = \pm\frac{1}{2}$, with the same sign chosen. Hence, we identify quasiparticles g_{\pm}^{++} and g_{\pm}^{--} , or g^+ , g^- in shortened notation (see Tab. 1).

Finally, the shrinking and growing of phase defect lines differs. When a wave back travels along a phase defect such that the tissue has recovered at both sides of the defect line, the phase defect line will retract. This implies that a tail and a pivot of same chirality travel together. We denote this as a “shrink” particle s_{\pm}^{\pm} , shortened s^{\pm} , and mark it in brown. Tab. 1 summarizes the, so far, discovered quasiparticles and their bound states in excitable media.

In the fourth step of our conceptual framework, we describe the evolution of these particles via diagrams similar to Feynman diagrams [Feynman, 1949]. For a first example, which represents the birth of a g^+ , g^- pair, after which the growth particles split into triples of head, tail, and pivot, see Fig. 1D f. In this graphical language, time passes from left to right and positions in space are represented along a single, vertical axis. The arrows represent the continuous existence of the quasiparticle in space and time, until an event happens in which the particle merges, splits or annihilates. Within this work, the diagrams already offer insight in the pattern’s dynamics, see the examples below.

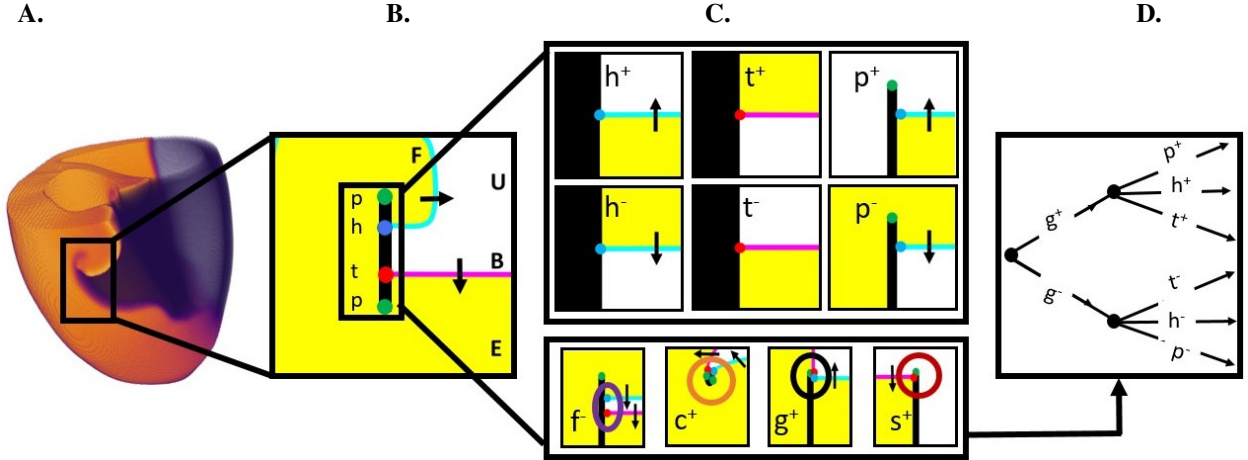


Figure 1: Conceptual framework for the analysis of excitation patterns using quasiparticles and Feynman diagrams. (A) A linear-core spiral wave [Bueno-Orovio et al., 2008] in a numerical simulation on a human biventricular geometry, see methods in Supp. Mat. 5. (B) Spatial analysis of the pattern, showing excited (E, yellow) and unexcited (U, white) regions. They are divided by the wave fronts (F, cyan), wave backs (B, magenta), and phase defect lines (black). The end points of these three different curves are topologically preserved as quasiparticles: heads (h, blue), tails (t, red), and pivots (p, green). (C) Top: Depending on the orientation, we assign positive or negative charges $Q = \pm \frac{1}{2}$ to heads and tails, and charges $P = \pm \frac{1}{2}$ to pivots. Bottom: Several combinations of head, tail, and pivot are seen to travel together through the medium, akin to bound states in particle physics: the classical tip ($f = h+t$), the spiral core ($c = h+t+2p$), and the newly identified phase defect growth sites ($g=h+t+p$), and shrinking sites ($s=t+p$) seen during arrhythmogenesis. For an overview of all quantities, see Table 1. (D) We propose to keep track of the recombinations of building blocks over time using Feynman-like diagrams.

3 Results

3.1 Figure of eight formation *in silico*

Fig. 2 shows a numerical simulation in the smoothed Karma model [Karma, 1993, Marcotte and Grigoriev, 2017] for atrial fibrillation, in which a single rotor spontaneously breaks up into multiple vortices. We analyze the creation of a vortex pair, labeled 2 and 3, away from a central persisting rotor, labeled 1, see the corresponding Feynman diagrams in panel B. When the wave front hits the wave back, a pair of g^+ , g^- emerges. Each particle lasts until the vortex makes a pivoting turn around the formed conduction block line, which marks the decay of the g -particles into a triple of head, tail, and pivot. Between $t = 160$ ms and 161 ms, the tail pair annihilates, as the wave back detaches from the conduction block line to form a single wave back again. The recovery of the tissue at the location of the initial collision marks the splitting of the phase defect line, which involves the birth of a shrink pair, just before $t = 168$ ms. Thereafter, both phase defect lines shrink until the head, tail, and two pivots are so close to each other that they effectively form a core particle.

3.2 Evolution of a break-up pattern *in silico*

In the regime of spiral break-up, which is thought to underlie cardiac fibrillation, the merging of two oppositely rotating spirals also takes place. Fig. 3 presents a detailed analysis using quasiparticles and Feynman diagrams. In the region of interest, there are initially two rotors at $t = 365$ ms, labeled 1 and 2. The annihilation of these rotors between times $t = 375$ ms and $t = 389$ ms is observed in the following steps:

The initial situation here consists of two rotors of opposite chirality, i.e. a c^+ , c^- pair. When they come close to each other, a tail pair is created at one of the conduction block lines at $t = 379$ ms. As the heads approach the space between the phase defects, a pair of growth particles is formed which close the gap between the separate rotor cores, such that the phase defects merge. After annihilation of the growth pair, we have only two pivots and two tails left. Each tail then turns around its pivot, creating shrink particles which reduce the length of the phase defect, causing it to vanish completely via annihilation of the shrink pair, just before $t = 389$ ms.

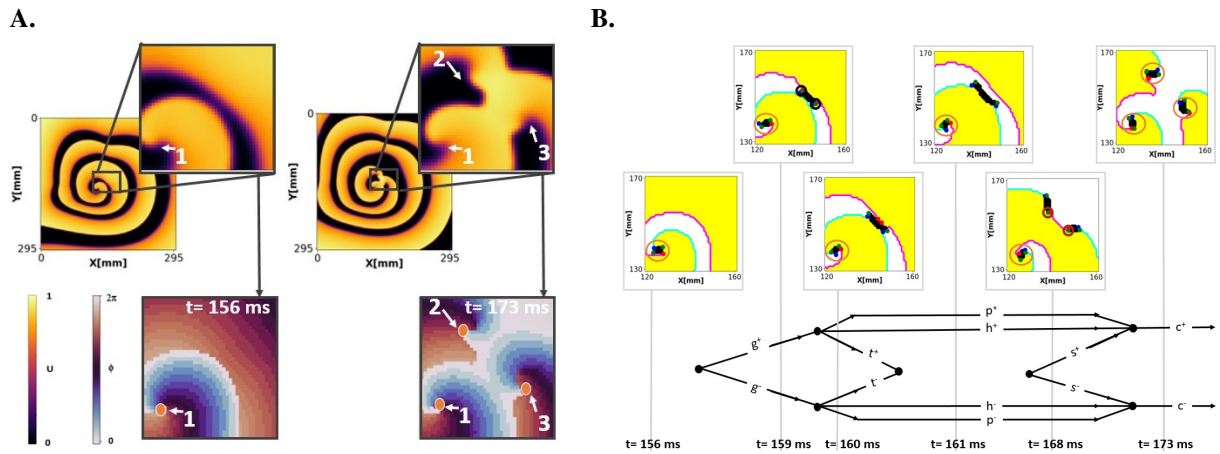


Figure 2: Feynman analysis of the creation of two spiral waves in a simulation of break-up [Karma, 1993, 1994]. (A) Two snapshots of the normalized transmembrane potential and corresponding phase maps [Gray et al., 1998, Kabus et al., 2022] with the apparent phase singularities highlighted. (B) Identification of the quasiparticles in subsequent snapshots showing that the birth of a rotor pair involves seven topological interactions, including the creation of a shrink pair, and the splitting of a conduction block line. No heads, tails or pivots are drawn at the boundary since it is an inset, not the medium boundary.

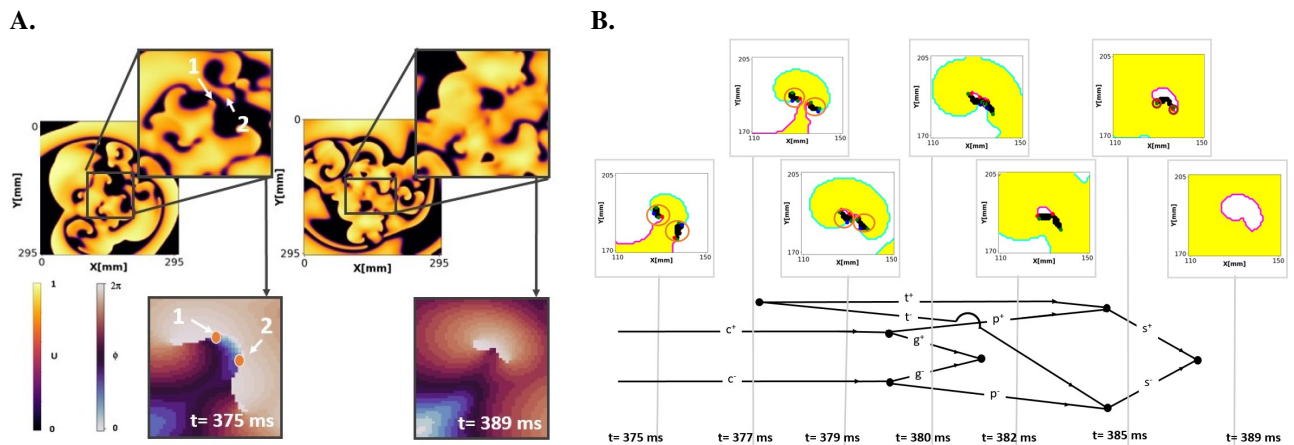


Figure 3: Feynman analysis of the annihilation of two spiral waves in a break-up simulation [Karma, 1993, 1994]. (A) Classical phase analysis shows the sudden vanishing of a phase singularity pair. (B) Feynman viewpoint, showing seven interactions including the birth of a tail pair, decay of core particles, merger of tail and pivot, and the annihilation of growth and shrink pairs.

Table 1: Overview of different particles, fundamental building blocks and bound states, together with their charges, notation, composition, and color code. In the extended notation, superscript denotes the head/tail charge Q in units of $\frac{1}{2}$ and subscripts denote the pivot charge P . As only quasiparticles of the same charge bind, the simplified notation indicates this with a single superscript \pm . The list is non-exhaustive and reflects our current knowledge.

particle	notation particle/charge	simplified notation particle/charge	charge Q	charge P	composition	color code
head	h^\pm	h^\pm	$\pm\frac{1}{2}$	0		
tail	t^\pm	t^\pm	$\pm\frac{1}{2}$	0		
pivot	p_\pm	p^\pm	0	$\pm\frac{1}{2}$		
filament; tip	$f^{\pm\pm}$	f^\pm	± 1	0	$h^\pm + t^\pm$	
core; phase singularity	$c_{\pm\pm}^{\pm\pm}$	c^\pm	± 1	± 1	$h^\pm + t^\pm + 2p_\pm$	
shrink site	s_\pm^\pm	s^\pm	$\pm\frac{1}{2}$	$\pm\frac{1}{2}$	$p_\pm + t^\pm$	
growth site	$g_\pm^{\pm\pm}$	g^\pm	± 1	$\pm\frac{1}{2}$	$h^\pm + t^\pm + p_\pm$	

3.3 Figure of eight creation *in vitro* under burst pacing

Fig. 4 shows the creation of a spiral pair in a monolayer of human atrial myocytes [Harlaar et al., 2021], see Appendix 5. By adding a voltage-sensitive dye to the culture, the local transmembrane voltage could be optically mapped [Salama et al., 1987], which is shown here after normalization to $[0, 1]$. The culture was stimulated at high frequency from the top left corner. After several transient wave breaks, i.e. conduction blocks, a pair of oppositely rotating spiral waves was formed, known in cardiology literature as a figure-of-eight re-entry [Wu et al., 1994]. The experiment presents an *in vitro* realization of the onset of an arrhythmia, an event to be prevented in patients.

Panel B of Fig 4 offers a thorough analysis via the quasiparticles and Feynman diagrams. As in the *in silico* case above, the initial conduction block produces a growth pair. Remarkably, the growth sites not only drift away from each other perpendicularly to the direction of the impeding wave, but when the wave back retracts, they make, roughly, a 90° turn and continue growing. Next, the heads make a pivoting turn and each growth site decays into triplets of (h^\pm, t^\pm, p^\pm) , leaving a single U-shaped phase defect line, see $t = 812$ ms. After the annihilation of the tail pair, the recovery of the initial zone of contact creates a shrink pair, which causes the splitting of the conduction block line. At $t = 823$ ms, the system has evolved to a state with two nearly parallel oriented conduction block lines, i.e. phase defects that comprise an effective functional isthmus around which a figure-of-eight rotor pair can revolve. When each of both shrink particles meets the head that moves through the isthmus, they briefly merge into a growth particle. Then, the pivots remain in place and the head and tail propagate along the phase defect line as an f -particle. In brief, the quasiparticle framework here reveals that the establishment of the figure-of-eight re-entry is a multi-step process, composed of nine fundamental interactions.

4 Discussion

A ‘standard model’ for excitation. The above analysis and examples show that complex excitation patterns can be described by three basic building blocks that form bound states. While tips and cores have been observed before, the growth and shrink of quasiparticles emerge from the framework itself. This situation is reminiscent of the ‘Standard Model’ in physics, which is based on a small set of fundamental particles [Mann, 2010] and explains almost all experimental results in particle physics. The ‘standard model for excitation patterns’ presented in this work gains its power from simple geometrical arguments, as the heads and tails are points where three zones meet, excited, unexcited, and phase defect.

Conservation laws. By construction, the Q -charges each sum to zero on any surface:

$$\sum_j Q_j^{\text{head}} = 0, \quad \sum_j Q_j^{\text{tail}} = 0. \quad (1)$$

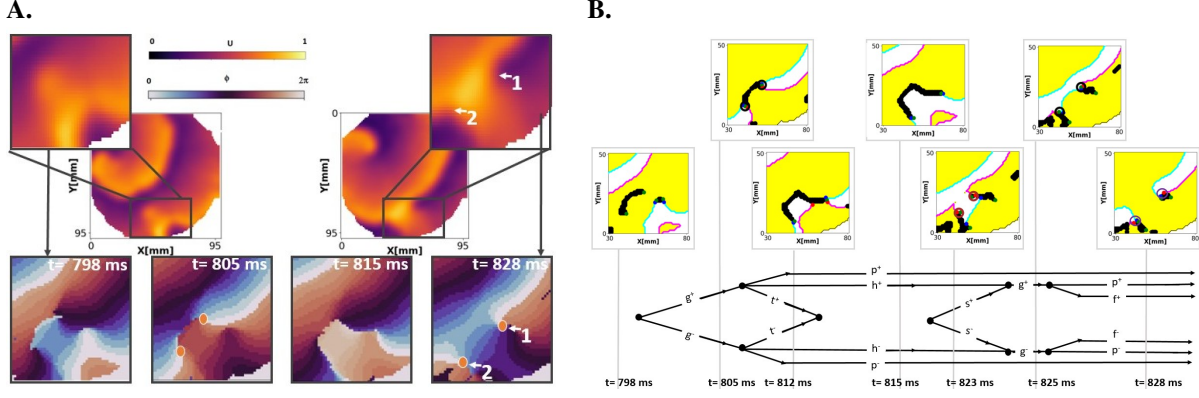


Figure 4: Feynman analysis of the creation of two spiral waves in an optical mapping experiment of a monolayer of human atrial myocytes [Harlaar et al., 2021]. (A) Classical phase analysis shows the creation, vanishing and recreation of a phase singularity pair. (B) Feynman analysis shows that both events are part of a single complex process occurring in nine steps. The formalism unifies the concepts of rotors and conduction block lines, and reveals how an initially flat conduction block line first takes a U-shape ($t = 812$ ms) and then becomes a functional isthmus around $t = 823$ ms.

Moreover, when summed over the closed border \mathcal{C} around a phase defect, they equal the classical topological charge [Goryachev and Kapral, 1996, Mermin, 1979] computed around a phase singularity:

$$\sum_{h \text{ on } \mathcal{C}} Q^h + \sum_{t \text{ on } \mathcal{C}} Q^t = Q^{\text{classical}} = \frac{1}{2\pi} \oint_{\mathcal{C}} \vec{\nabla} \phi \cdot d\vec{\ell}. \quad (2)$$

These relations are not specific to the heart, as heads and tails could be present in any medium with non-linear switching behavior, e.g. epidemic spread, oscillatory media in chemistry and biology and front propagation in meteorology or network science.

When a wave front is stopped by unrecovered elements in such systems, a conduction block line arises, whose endpoints we state to carry a pivot charge $P = \pm \frac{1}{2}$. However, when a phase defect grows hitting the medium boundary and then shrinks, it can disappear altogether, such that the total P -charge in the medium is not conserved in time. As an example, a single linear-core rotor in a bounded geometry will have $P = \pm 1$. The classical theory of phase singularities [Clayton et al., 2005] does not distinguish between P and Q -charges, which is also not necessary in the small-core regime.

Dynamical transitions. The motivation for this study was to investigate the interactions between short-lived rotors and approaching wave fronts during arrhythmogenesis [Clayton et al., 2005]. We go beyond the observation that apparent phase singularities co-locate with conduction blocks [Rodrigo et al., 2017, Arno et al., 2021], by looking at a finer spatial scale. We discovered multiple interactions of the quasiparticles in the data and represented them schematically. Our initial analyses show new mechanistic insight, like the dynamical isthmus formation in Fig. 4. It can be expected that the automated construction of those diagrams for larger fibrillation domains (see Fig. 3) will allow an enhanced classification and characterization of those patterns.

Links between particle physics and cardiology. The establishment of a “standard model for arrhythmias” allows us to introduce even more concepts from particle physics in the world of excitable media. First, since cardiac tissue is in reality non-homogeneous, a wave front will often create a head pair near obstacles, e.g. areas of fibrosis, which annihilates shortly afterwards. Such a phenomenon is similar to the creation and annihilation of particle-antiparticle pairs in physics. Second, the difference between linear-core and circular-core rotors follows from the mutual interaction between pivots, which can be expressed with spiral wave response functions [Biktasheva and Biktashev, 2003, Marcotte and Grigoriev, 2016, Dierckx et al., 2017]. If nearby pivot charges of the same charge attract each other, they form a core particle. Conversely, when they repel each other, a linear-core rotor emerges. However, such a phase defect cannot grow larger than the width of a traveling pulse in the medium, since otherwise the defect line will break by the creation of a new p_+ , p_- pair. Therefore, pivot particles are subjected to confinement, analogous to quarks in quantum chromodynamics [Wilson, 1974].

Finally, note that in Fig. 1B, there is an apparent symmetry: When excited regions are hypothetically swapped with the unexcited ones, the heads become tails and the arrow of time is reversed. However, this symmetry is explicitly broken since the growth and decay of phase defect lines occurs via different quasiparticles, namely the growth and shrink sites. *Limitations.* The local state of a cell was here assumed to lie along a cycle, such that it can be labeled with a single

phase variable $\phi(\vec{r}, t)$. Capturing specific memory effects, such as alternans [Karma, 1994] or after-depolarizations in cardiac tissue [Weiss et al., 2010] will require an extension of the formalism.

Applications to cardiac arrhythmia. The above examples revealed dynamics at a smaller scale in space and time than the phase singularity picture. Conducting similar analysis on existing datasets during arrhythmias is likely to give new clues on underlying mechanisms. More specifically, counting the elementary interactions [Marcotte and Grigoriev, 2017], computing statistics of potentially large Feynman diagrams, and deriving interaction laws between the quasiparticles could prove useful.

The heads and tails directly relate the electrical signals recorded within the heart or on the body surface by clinicians. In good approximation, the unipolar electrical potential measured by an electrode is determined by the angle subtended by the wave fronts and wave backs, seen from the electrode [Holland and Arnsdorf, 1977]. The measured signal is thus only determined by the boundaries of the wave fronts and backs, namely the heads and tail curves in three dimensions. Therefore, the concepts of heads and tails may also prove useful when improving efficient inverse methods to recover spatio-temporal activation sequences from patient measurements [Ramanathan et al., 2004].

The pivot sites, termed quasiparticles here, are actively being investigated by clinicians as possible ablation targets [Seitz et al., 2017]. We believe that the analysis of the clinical data and the pivot ablation within our framework can help to answer if, why, and when these points are appropriate ablation targets.

Outlook. Another application of this framework is to characterize more processes in terms of elementary interactions [Marcotte and Grigoriev, 2017]. Our diagrams can potentially be used for predictive calculations, like for the critical size of a wave break, or the timescale at which a rotor produces multiple wavelets. In three spatial dimensions, the heads, tails, and pivots become string-like objects, refining the concept of a rotor filament [Winfree, 1973, Clayton et al., 2005]. As we provide an analysis method rather than a theoretical “model”, it can be applied to any excitable surface pattern that is sufficiently sampled in space and time.

5 Conclusion

We presented a conceptual framework revising the classical theory of arrhythmia patterns, intentionally designed for regimes that are clinically observed during complex arrhythmias: short-lived pivoting motion and prominent conduction blocks. By classifying the end points of wave fronts, wave backs and conduction blocks as charged quasiparticles, Feynman-like diagrams can be created from phase maps or local activation times. We believe this framework has the potential to become a useful analysis tool for cardiac patterns, and perhaps also beyond the cardiac electrophysiology context.

Funding

L. Arno is funded by a FWO-Flanders fellowship, grant 117702N. D. Kabus is supported by KU Leuven grant GPUL/20/012. H. Dierckx was supported by KU Leuven grant ST/019/007.

Acknowledgments

The authors are grateful to D.A. Pijnappels, A.A.F. de Vries and N. Harlaar for collecting and sharing the hiAM dataset. The authors thank J. Ector for helpful discussions. The authors thank A.A.F. de Vries for useful comments on the manuscript.

Author contribution statements

L.A. contributed to the numerical simulations, data analysis, scientific discussions and writing of the manuscript. D.K. contributed to the data analysis methods, scientific discussions, simulation software and writing of the manuscript. H.D. contributed to the central idea of using quasiparticles and Feynman diagrams, simulation software, scientific discussions and writing of the manuscript. Correspondence and requests for materials should be addressed to Hans Dierckx.

Data and Code availability

The numerical methods implemented for this paper are available as a Python module at https://gitlab.com/heartkor/py_ithildin, see also [Kabus et al., 2022]. The Python scripts used to generate the figures in this

paper are available at https://gitlab.com/heartkor/pd_diagrams. Finally, we have published the simulation output and pre-processed optical voltage mapping data on which the scripts were applied on Zenodo DOI: [doi:10.5281/zenodo.8107271](https://doi.org/10.5281/zenodo.8107271). This archive also contains the Python module and scripts.

Methods

In silico data generation. The synthetic data from Fig. 1A were obtained by Euler-forward stepping of the Bueno-Orovio-Cherry-Fenton model [Bueno-Orovio et al., 2008], with step size 0.31 mm and time step 0.1 ms in a biventricular heart geometry. The fibrillation-like data from Fig. 3 were obtained by Euler-forward stepping of the Karma model [Karma, 1993, 1994] modified according to Marcotte et al. [Marcotte and Grigoriev, 2017], with step size 1 mm and time step 0.1 ms.

Experimental data generation. Monolayers of fully functional human atrial myocytes were generated as described in detail by Harlaar et al. [Harlaar et al., 2021]. A voltage-sensitive dye was added to the culture, after which a real-time recording can be made of the intensity of emitted light, which is a measure of the local transmembrane potential [Salama et al., 1987]. The recording has a resolution of 100×100 pixels with pixel size 0.25 mm. The sampling time between frames was 6 ms.

Data analysis. Local activation times were converted to phase as done by Kabus *et al.* 2022 [Kabus et al., 2022] with time constant $\tau = 30$ ms. Wave fronts and backs were selected as isochrones of constant phase $\phi_{\text{front}} = 1$ rad and $\phi_{\text{back}} = 5$ rad. Phase defects were tracked as the points for which the phase coherence [Kabus et al., 2022] is above the threshold 0.5. The positions of heads, tails, pivots and compound particles were drawn manually on the resulting figures.

References

- WHO. The top 10 causes of death., 2020. URL <https://www.who.int/news-room/fact-sheets/detail/the-top-10-causes-of-death>.
- Miguel Rodrigo, Andreu M. Climent, Alejandro Liberos, Francisco Fernandez-Avilas, Omer Berenfeld, Felipe Atienza, and Maria S. Guillem. Technical considerations on phase mapping for identification of atrial reentrant activity in direct- and inverse-computed electrograms. *Circulation: Arrhythmia and Electrophysiology*, 10(9):e005008, 2017.
- Paul B. Tabereaux, Derek J. Dossdall, and Raymond E. Ideker. Mechanisms of VF maintenance: Wandering wavelets, mother rotors, or foci. *Heart Rhythm*, 6(3):405–415, March 2009. ISSN 15475271. doi:10.1016/j.hrthm.2008.11.005. URL <https://linkinghub.elsevier.com/retrieve/pii/S1547527108010886>.
- Julien Seitz, Clément Bars, Guillaume Théodore, Sylvain Beurtheret, Nicolas Lellouche, Michel Bremond, Ange Ferracci, Jacques Faure, Guillaume Penaranda, Masatoshi Yamazaki, Uma Mahesh R. Avula, Laurence Curel, Sabrina Siame, Omer Berenfeld, André Pisapia, and Jérôme Kalifa. AF Ablation Guided by Spatiotemporal Electrogram Dispersion Without Pulmonary Vein Isolation. *Journal of the American College of Cardiology*, 69(3):303–321, January 2017. ISSN 07351097. doi:10.1016/j.jacc.2016.10.065. URL <https://linkinghub.elsevier.com/retrieve/pii/S0735109716370796>.
- R. P. Feynman. The Theory of Positrons. *Physical Review*, 76(6):749–759, September 1949. ISSN 0031-899X. doi:10.1103/PhysRev.76.749. URL <https://link.aps.org/doi/10.1103/PhysRev.76.749>.
- M. Haissaguerre, P. Jais, D. Shah, A. Takahashi, M. Hocini, G. Quiniou, S. Garrigue, A. Le Mouroux, Le Metayer P, and Clementy J. Spontaneous initiation of atrial fibrillation by ectopic beats originating in the pulmonary veins. *New England Journal of Medicine*, 339:659–666, 1998.
- Edmond M Cronin, Frank M Bogun, Philippe Maury, Petr Peichl, Minglong Chen, Narayanan Namboodiri, Luis Aguinaga, Luiz Roberto Leite, Sana M Al-Khatib, Elad Anter, Antonio Berruezo, David J Callans, Mina K Chung, Phillip Cuculich, Andre d’Avila, Barbara J Deal, Paolo Della Bella, Thomas Deneke, Timm-Michael Dickfeld, Claudio Hadid, Haris M Haqqani, G Neal Kay, Rakesh Latchamsetty, Francis Marchlinski, John M Miller, Akihiko Nogami, Akash R Patel, Rajeev Kumar Pathak, Luis C Sáenz Morales, Pasquale Santangeli, John L Sapp, Andrea Sarkozy, Kyoko Soejima, William G Stevenson, Usha B Tedrow, Wendy S Tzou, Niraj Varma, Katja Zeppenfeld, ESC Scientific Document Group, Samuel J Asirvatham, Eduardo Back Sternick, Janice Chyou, Sabine Ernst, Guilherme Fenelon, Edward P Gerstenfeld, Gerhard Hindricks, Koichi Inoue, Jeffrey J Kim, Kousik Krishnan, Karl-Heinz Kuck, Martin Ortiz Avalos, Thomas Paul, Mauricio I Scanavacca, Roderick Tung, Jamie Voss, Takumi Yamada, and Teiichi Yamane. 2019 HRS/EHRA/APHRS/LAHRS expert consensus statement on catheter ablation of ventricular arrhythmias. *EP Europace*, 21(8):1143–1144, August 2019. ISSN 1099-5129, 1532-2092. doi:10.1093/europace/euz132. URL <https://academic.oup.com/europace/article/21/8/1143/5487880>.
- Nebojša Mujović, Milan Marinković, Radoslaw Lenarczyk, Roland Tilz, and Tatjana S. Potpara. Catheter Ablation of Atrial Fibrillation: An Overview for Clinicians. *Advances in Therapy*, 34(8):1897–1917, August 2017. ISSN 0741-238X, 1865-8652. doi:10.1007/s12325-017-0590-z. URL <http://link.springer.com/10.1007/s12325-017-0590-z>.
- R.A. Gray, A.M. Pertsov, and J. Jalife. Spatial and temporal organization during cardiac fibrillation. *Nature*, 392:75–78, 1998.
- J. Jalife, R.A. Gray, G.E. Moeley, and J.M. Davidenko. Self-organization and the dynamical nature of ventricular fibrillation. *Chaos*, 8:79–93, 1998.
- Alexander Samol, Kathrin Hahne, and Gerold Monnig. Atrial fibrillation and silent stroke: Links, risks, and challenges. *Vascular Health and Risk Management*, 2016:65, 2016. doi:10.2147/VHRM.S81807.
- M.A. Allesie, F.I.M. Bonke, and F.J.G. Schopman. Circus movement in rabbit atrial muscle as a mechanism of tachycardia. *Circ. Res.*, 33:54–62, 1973.
- R.A. Gray, J. Jalife, A. Panfilov, W.T. Baxter, C. Cabo, and A.M. Pertsov. Non-stationary vortex-like reentrant activity as a mechanism of polymorphic ventricular tachycardia in the isolated rabbit heart. *Circulation*, 91:2454–2469, 1995.
- G.K. Moe and J.A. Abildskov. Atrial fibrillation as a self-sustained arrhythmia independent of focal discharge. *Am. Heart J.*, 58:59–70, 1959.
- Seungyup Lee, Celeen M. Khrestian, Jayakumar Sahadevan, and Albert L. Waldo. Reconsidering the multiple wavelet hypothesis of atrial fibrillation. *Heart Rhythm*, 17(11):1976–1983, November 2020. ISSN 15475271. doi:10.1016/j.hrthm.2020.06.017. URL <https://linkinghub.elsevier.com/retrieve/pii/S1547527120305956>.
- L. Arno, J. Quan, N.T. Nguyen, M. Vanmarcke, E.G. Tolkacheva, and H. Dierckx. A phase defect framework for the analysis of cardiac arrhythmia patterns. *Front. Physiol.*, 12, 2021.

- Kedar K. Aras, Matthew W. Kay, and Igor R. Efimov. Ventricular Fibrillation: Rotors or Foci? Both! *Circulation: Arrhythmia and Electrophysiology*, 10(12):e006011, December 2017. ISSN 1941-3149, 1941-3084. doi:10.1161/CIRCEP.117.006011. URL <https://www.ahajournals.org/doi/10.1161/CIRCEP.117.006011>.
- Nitaro Shibata, Shin Inada, Kazuo Nakazawa, Takashi Ashihara, Naoki Tomii, Masatoshi Yamazaki, Haruo Honjo, Hiroshi Seno, and Ichiro Sakuma. Mechanism of Ventricular Fibrillation: Current Status and Problems. *Advanced Biomedical Engineering*, 11(0):117–135, 2022. ISSN 2187-5219. doi:10.14326/abe.11.117. URL https://www.jstage.jst.go.jp/article/abe/11/0/11_11_117/_article.
- R.H. Clayton, E.A. Zhuchkova, and A.V. Panfilov. Phase singularities and filaments: Simplifying complexity in computational models of ventricular fibrillation. *Prog Biophys Molec Biol*, 90:378–398, 2005.
- M-A. Bray and J.P. Wikswo. Examination of optical depth effects on fluorescence imaging of cardiac propagation. *Biophys. J.*, 85:4134–4145, 2003.
- Sanjiv M. Narayan, David E. Krummen, Kalyanam Shivkumar, Paul Clopton, Wouter-Jan Rappel, and John M. Miller. Treatment of atrial fibrillation by the ablation of localized sources. *Journal of the American College of Cardiology*, 60(7):628–636, August 2012. ISSN 07351097.
- A.V. Panfilov and H. Dierckx. *Theory of Cardiac Arrhythmias*, pages 325–335. Elsevier, London, 2017.
- N. Tomii, M. Yamazaki, T. Ashihara, K. Nakazawa, N. Shibata, H. Honjo, and I. Sakuma. Spatial phase discontinuity at the center of moving cardiac spiral waves. *Computers in Biology and Medicine*, 130, 2021.
- M.J. Janse, F.J.L. van Capelle, H. Morsink, A.G. Kleber, F.J.G. Wilms-Schopman, R. Cardinal, C. Naumann D’Alnoncourt, and D. Durrer. Flow of injury current and patterns of excitation during early ventricular arrhythmias in acute regional myocardial ischemia in isolated porcine and canine hearts. Evidence for 2 different arrhythmogenic mechanisms. *Circulation Research*, 47:151–165, 1980.
- V.I. Krinsky, I.R. Efimov, and J. Jalife. Vortices with linear cores in excitable media. *Proc. Roy. Soc. London A*, 437, 1992.
- A.T. Winfree, S. Caudle, G.I. Chen, P. McGuire, and Z. Szilagyi. Quantitative optical tomography of chemical waves and their organizing centers. *Chaos: An Interdisciplinary Journal of Nonlinear Science*, 12, 1996.
- A. Bueno-Orovio, E.M. Cherry, and F.H. Fenton. Minimal model for human ventricular action potentials in tissue. *J Theor Biol*, 253:544–560, 2008.
- A. Karma. Spiral breakup in model equations of action potential propagation in cardiac tissue. *Physical review letters*, 7, 1993.
- C. D. Marcotte and R. O. Grigoriev. Dynamical mechanism of atrial fibrillation: A topological approach. *Chaos: An Interdisciplinary Journal of Nonlinear Science*, 27:093936, 2017.
- A. Karma. Electrical alternans and spiral wave breakup in cardiac tissue. *Chaos: An Interdisciplinary Journal of Nonlinear Science*, 3, 1994.
- D. Kabus, L. Arno, L. Leenknegt, A.V. Panfilov, D.A. Pijnappels, and H. Dierckx. Numerical methods for the detection of phase defect structures in excitable media. *PLOS ONE*, 2022.
- N. Harlaar, S. O. Dekker, J. Zhang, R. R. Snabel, M. W. Veldkamp, A. O. Verkerk, C. C. Fabres, V. Schwach, L. J. S. Lerink, M. R. Rivaud, A. A. Mulder, W. E. Corver, M. J. T. H. Goumans, D. Dobrev, R. J. M. Klautz, M. J. Schalijs, G. J. C. Veenstra, R. Passier, T. J. van Brakel, D. A. Pijnappels, and A. A. F. de Vries. Conditional immortalization of human atrial myocytes for the generation of in vitro models of atrial fibrillation. *Nature Biomedical Engineering*, 2021.
- G. Salama, R. Lombardi, and J. Elson. Maps of optical action potentials and nadh fluorescence in intact working hearts. *Am. J. Physiol. Heart Circ. Physiol.*, 252:H384–H394, 1987.
- Delon Wu, San-Jou Yeh, Chun-Chieh Wang, Ming-Shien Wen, and Fun-Chung Lin. Double loop figure-of-8 reentry as the mechanism of multiple atrioventricular node reentry tachycardias. *American Heart Journal*, 127(1):83–95, January 1994. ISSN 00028703. doi:10.1016/0002-8703(94)90513-4. URL <https://linkinghub.elsevier.com/retrieve/pii/0002870394905134>.
- R. Mann. *An Introduction to Particle Physics and the Standard Model*. CRC Press, Boca Raton, 2010. doi:10.1201/9781420083002.
- Andrei Goryachev and Raymond Kapral. Spiral Waves in Chaotic Systems. *Physical Review Letters*, 76(10):1619–1622, March 1996. ISSN 0031-9007, 1079-7114. doi:10.1103/PhysRevLett.76.1619. URL <https://link.aps.org/doi/10.1103/PhysRevLett.76.1619>.

- N. D. Mermin. The topological theory of defects in ordered media. *Reviews of Modern Physics*, 51(3):591–648, July 1979. ISSN 0034-6861. doi:10.1103/RevModPhys.51.591. URL <https://link.aps.org/doi/10.1103/RevModPhys.51.591>.
- I.V. Biktasheva and V.N. Biktashev. Wave-particle dualism of spiral wave dynamics. *Phys. Rev. E*, 67:026221, 2003.
- C. D. Marcotte and R. O. Grigoriev. Adjoint eigenfunctions of temporally recurrent single-spiral solutions in a simple model of atrial fibrillation. *Chaos: An Interdisciplinary Journal of Nonlinear Science*, 26(9):093107, 2016. URL <http://aip.scitation.org/doi/abs/10.1063/1.4962644>.
- H. Dierckx, H. Verschelde, and A.V. Panfilov. Measurement and structure of spiral wave response functions. *Chaos*, 27:093912 1–10, 2017.
- Kenneth G. Wilson. Confinement of quarks. *Physical Review D*, 10(8):2445–2459, October 1974. ISSN 0556-2821. doi:10.1103/PhysRevD.10.2445. URL <https://link.aps.org/doi/10.1103/PhysRevD.10.2445>.
- James N. Weiss, Alan Garfinkel, Hrayr S. Karagueuzian, Peng-Sheng Chen, and Zhilin Qu. Early Afterdepolarizations and Cardiac Arrhythmias. *Heart rhythm : the official journal of the Heart Rhythm Society*, 7(12):1891, December 2010. doi:10.1016/j.hrthm.2010.09.017. URL <https://www.ncbi.nlm.nih.gov/pmc/articles/PMC3005298/>. Publisher: NIH Public Access.
- Roger P Holland and Morton F Arnsdorf. Solid angle theory and the electrocardiogram: physiologic and quantitative interpretations. *Progress in Cardiovascular diseases*, 19(6):431–457, 1977.
- Charulatha Ramanathan, Raja N Ghanem, Ping Jia, Kyungmoo Ryu, and Yoram Rudy. Noninvasive electrocardiographic imaging for cardiac electrophysiology and arrhythmia. *Nature Medicine*, 10(4):422–428, April 2004. ISSN 1078-8956, 1546-170X. doi:10.1038/nm1011. URL <http://www.nature.com/articles/nm1011>.
- A.T. Winfree. Scroll-shaped waves of chemical activity in three dimensions. *Science*, 181:937–939, 1973.